Measurements of the Electric Form Factor of the Neutron up to $Q^2 = 3.4$ GeV^2 using the Reaction $^3\overrightarrow{\text{He}}(\vec{e}, e'n)pp$

S. Riordan,[1,2,3] S. Abrahamyan,[4] B. Craver,[2] A. Kelleher,[5] A. Kolarkar,[6] J. Miller,[7] G.D. Cates,[2] N. Liyanage,[2] B. Wojtsekhowski,[8,*] A. Acha,[9] K. Allada,[6] B. Anderson,[10] K.A. Aniol,[11] J.R.M. Annand,[12] J. Arrington,[13] T. Averett,[5] A. Beck,[14,8] M. Bellis,[1] W. Boeglin,[9] H. Breuer,[7] J.R. Calarco,[15] A. Camsonne,[8] J.P. Chen,[8] E. Chudakov,[8] L. Coman,[9] B. Crowe,[16] F. Cusanno,[17] D. Day,[2] P. Degtyarenko,[8] P.A.M. Dolph,[2] C. Dutta,[6] C. Ferdi,[18] C. Fernández-Ramírez,[19] R. Feuerbach,[8,5] L.M. Fraile,[19] G. Franklin,[1] S. Frullani,[17] S. Fuchs,[5] F. Garibaldi,[17] N. Gevorgyan,[4] R. Gilman,[20,8] A. Glamazdin,[21] J. Gomez,[8] K. Grimm,[5] J.-O. Hansen,[8] J.L. Herraiz,[19] D.W. Higinbotham,[8] R. Holmes,[22] T. Holmstrom,[5] D. Howell,[23] C.W. de Jager,[8] X. Jiang,[20] M.K. Jones,[8] J. Katich,[5] L.J. Kaufman,[3] M. Khandaker,[24] J.J. Kelly,[7,†] D. Kiselev,[25] W. Korsch,[6] J. LeRose,[8] R. Lindgren,[2] P. Markowitz,[9] D.J. Margaziotis,[11] S. May-Tal Beck,[14,8] S. Mayilyan,[4] K. McCormick,[26] Z.-E. Meziani,[27] R. Michaels,[8] B. Moffit,[5] S. Nanda,[8] V. Nelyubin,[2] T. Ngo,[11] D.M. Nikolenko,[28] B. Norum,[2] L. Pentchev,[5] C.F. Perdrisat,[5] E. Piasetzky,[29] R. Pomatsalyuk,[21] D. Protopopescu,[12] A.J.R. Puckett,[14] V.A. Punjabi,[24] X. Qian,[30] Y. Qiang,[14] B. Quinn,[1] I. Rachek,[28] R.D. Ransome,[20] P.E. Reimer,[13] B. Reitz,[8] J. Roche,[8] G. Ron,[29] O. Rondon,[2] G. Rosner,[12] A. Saha,[8] M.M. Sargsian,[9] B. Sawatzky,[27] J. Segal,[8] M. Shabestari,[2] A. Shahinyan,[4] Yu. Shestakov,[28] J. Singh,[2] S. Širca,[14] P. Souder,[22] S. Stepanyan,[31] V. Stibunov,[32] V. Sulkosky,[5] S. Tajima,[2] W.A. Tobias,[2] J.M. Udias,[19] G.M. Urciuoli,[17] B. Vlahovic,[16] H. Voskanyan,[4] K. Wang,[2] F.R. Wesselmann,[24] J.R. Vignote,[33] S.A. Wood,[8] J. Wright,[26] H. Yao,[27] and X. Zhu[14]

[1]*Carnegie Mellon University, Pittsburgh, PA 15213*
[2]*University of Virginia, Charlottesville, VA 22903*
[3]*University of Massachusetts, Amherst, MA 01003*
[4]*Yerevan Physics Institute, Yerevan 375036, Armenia*
[5]*College of William and Mary, Williamsburg, VA 23187*
[6]*University of Kentucky, Lexington, KY 40506*
[7]*University of Maryland, College Park, MD 20742*
[8]*Thomas Jefferson National Accelerator Facility, Newport News, VA 23606*
[9]*Florida International University, Miami, FL 33199*
[10]*Kent State University, Kent, OH 44242*
[11]*California State University Los Angeles, Los Angeles, CA 90032*
[12]*University of Glasgow, Glasgow G12 8QQ, Scotland, U.K.*
[13]*Physics Division, Argonne National Laboratory, Argonne, IL 60439*
[14]*Massachusetts Institute of Technology, Cambridge, MA 02139*
[15]*University of New Hampshire, Durham, NH 03824*
[16]*North Carolina Central University, Durham, NC 27707*
[17]*INFN gr. Sanità coll. Sezione di Roma and Istituto Superiore di Sanità, Rome, Italy*
[18]*Université Blaise Pascal/IN2P3, F-63177 Aubière, France*
[19]*Universidad Complutense de Madrid, Madrid, Spain*
[20]*Rutgers, The State University of New Jersey, Piscataway, NJ 08854*
[21]*Kharkov Institute of Physics and Technology, Kharkov 61108, Ukraine*
[22]*Syracuse University, Syracuse, NY 13244*
[23]*University of Illinois, Urbana-Champaign, IL 61801*
[24]*Norfolk State University, Norfolk, VA 23504*
[25]*Universität Basel, CH-4056 Basel, Switzerland*
[26]*Old Dominion University, Norfolk, VA 23529*
[27]*Temple University, Philadelphia, PA 19122*
[28]*Budker Institute for Nuclear Physics, Novosibirsk 630090, Russia*
[29]*Tel Aviv University, Tel Aviv, 69978 Israel*
[30]*Duke University and TUNL, Durham, NC 27708*
[31]*Kyungpook National University, Taegu City, South Korea*
[32]*Institute for Nuclear Physics, Tomsk 634050, Russia*
[33]*Instituto de Estructura de la Materia, Madrid, Spain*
(Dated: October 23, 2010)

The electric form factor of the neutron was determined from studies of the reaction $^3\overrightarrow{\text{He}}(\vec{e}, e'n)pp$ in quasi-elastic kinematics in Hall A at Jefferson Lab. Longitudinally polarized electrons were scattered off a polarized target in which the nuclear polarization was oriented perpendicular to the momentum transfer. The scattered electrons were detected in a magnetic spectrometer in coincidence with neutrons that were registered in a large-solid-angle detector. More than doubling

the Q^2-range over which it is known, we find $G_E^n = 0.0236 \pm 0.0017(stat) \pm 0.0026(syst)$, $0.0208 \pm 0.0024 \pm 0.0019$, and $0.0147 \pm 0.0020 \pm 0.0014$ for $Q^2 = 1.72$, 2.48, and 3.41 GeV^2, respectively.

PACS numbers: 14.20.Dh, 13.40.Gp, 24.70.+s, 25.30.Bf

Understanding the nucleon in terms of QCD degrees of freedom requires precision measurements of nucleon structure, including the form factors (FFs) that govern the elastic scattering of electrons. Important advances in such efforts came from the determination, at Jefferson Lab (JLab), of the ratio of the electric and magnetic elastic FFs of the proton, G_E^p/G_M^p, over a range of the negative four-momentum transfer squared (Q^2) of 1 to 6 GeV^2 [1]. The ratio G_E^p/G_M^p was observed to decrease almost linearly with increasing Q^2, when expectations, based on both earlier cross-section measurements and prevailing theoretical models of the nucleon, had been that such a ratio is constant. This observation has clarified the necessity for a reconsideration of nucleon structure with an increased emphasis on the significance of quark orbital angular momentum (OAM), see e.g. the review [2]. Evidence of quark OAM has subsequently been observed in several other independent contexts [3]. Given the important implications of Ref. [1], it is critical to determine the neutron form-factor ratio, G_E^n/G_M^n, in a Q^2-region where the unexpected results for the proton were observed, and thus test the theoretical explanations that have emerged for the proton data.

The powerful method of determining FFs using double-polarization asymmetries [4], which led to the striking results of [1], has also been used to study $g_n = \mu_n G_E^n/G_M^n$, where $\mu_n = -1.913$ is the neutron magnetic moment, up to $Q^2 = 1.5$ GeV^2. These experiments have employed polarized electrons and either a neutron polarimeter [5, 6], a polarized deuteron target [7, 8], or a polarized ^{3}He target [9–12]. At low momentum transfer, the nuclear effects in double-polarization asymmetries have been taken into account using precise non-relativistic calculations of ^{3}He based on the Faddeev-like integral equations [13], whereas at large Q^2 the eikonal approximation [14] provides sufficient precision. For Q^2-values of several GeV^2, even polarization-based studies of g_n become very challenging due to the small cross sections involved, thus necessitating significant technical development.

We report a measurement of g_n, up to $Q^2 = 3.4$ GeV^2, performed at JLab in experimental Hall A. The experiment was made possible through the use of a high-luminosity optically-polarized ^{3}He target, a magnetic spectrometer of 76 msr solid angle to detect the scattered electrons, and a large neutron detector with matched acceptance. The typical ^{3}He-electron luminosity was 5×10^{35} cm^{-2}/s. The central kinematics, as well as the average values of various experimental parameters, are listed in Table I.

The experiment, E02-013, used a longitudinally polarized electron beam with a current of 8 μA. The helicity

TABLE I: Kinematics and other parameters of the experiment: the negative four-momentum transfer, Q^2; the rms of Q^2 range, ΔQ^2; beam energy, E$_{\text{beam}}$; central angle of the electron spectrometer, θ_{e}; central angle of the neutron detector, θ_{n}; distance from the target to the neutron detector, D; longitudinal beam polarization, P_{e}; target polarization, P_{He}.

$\langle Q^2 \rangle$	[GeV^2]	1.72	2.48	3.41
ΔQ^2	[GeV^2]	0.14	0.18	0.22
E$_{\text{beam}}$	[GeV]	2.079	2.640	3.291
θ_{e}	[deg]	51.6	51.6	51.6
θ_{n}	[deg]	33.8	29.2	24.9
D	[m]	8.3	11	11
$\langle P_{\text{e}} \rangle$	[%]	85.2	85.0	82.9
$\langle P_{\text{He}} \rangle$	[%]	47.0	43.9	46.2

of the beam was pseudo-randomly flipped at a rate of 30 Hz. The helicity-correlated charge asymmetry was monitored and kept below 0.01%. The beam polarization, monitored continuously by a Compton polarimeter, and measured several times by a Møller polarimeter [15], was determined with a relative accuracy of 3%.

The polarized ^{3}He target, while similar in many respects to the target described in Ref. [15], included several important improvements. The ^{3}He was polarized by spin-exchange with an optically pumped alkali vapor, but unlike earlier targets at JLab, the alkali vapor was a mixture of Rb and K [16], rather than Rb alone. This greatly increased the efficiency of spin transfer to the ^{3}He nuclei, resulting in a significantly higher polarization. The ^{3}He gas (at a pressure of $\sim$10 atm), a 1% admixture of N$_2$ (to aid in the optical pumping process), and the alkali vapor were contained in a sealed glass cell with two chambers. The portion of the cell in the electron beam was a cylinder 40 cm in length and 2 cm in diameter. The polarization of the target was measured every six hours using NMR method, with a relative accuracy of 4.7%, and was calibrated using a technique based on electron paramagnetic resonance [17]. A magnetic field of 25 G was created in the target area by means of a 100 cm gap dipole magnet. The horizontal direction of the field in the target area, 118° with respect to the electron beam, was nearly orthogonal to the momentum-transfer vector and was measured to 1 mrad accuracy over the length of the target. The target cell alignment along the beam was regularly checked by varying the size of the electron beam spot. The background from beam-cell interaction was estimated using data collected with an empty cell and was found to be negligible.

The scattered electrons were detected in the BigBite spectrometer, originally used at NIKHEF-K [18]. It

consisted of a dipole magnet and a detector stack subtending a solid angle of 76 msr for a 40 cm long target. For this experiment, the detector package was completely rebuilt to accommodate an increase in luminosity of 10^5. The spectrometer was equipped with 15 planes of high-resolution multi-wire drift chambers, a two-layer lead-glass calorimeter for triggering and pion rejection, and a scintillator hodoscope for event timing information. BigBite provided a relative momentum resolution of $\sim$1% for electrons with a momentum of 1.5 GeV/c, a time resolution of 0.25 ns, and an angular resolution of 0.3 (0.7) mrad in the vertical (horizontal) direction. The Q^2-acceptance was $\sim$10% of the Q^2-value despite the large angular acceptance of BigBite, thanks to its large 5:1 vertical/horizontal aspect ratio.

The recoiling nucleons were detected in coincidence using a large hadron detector, BigHAND, that included (moving away from the target) two planes of segmented veto counters, a 2.5 cm lead shield, and seven layers of neutron counters. Each neutron-counter layer covered a $1.7 \times 4 \, \text{m}^2$ area and was comprised of 25(40) plastic scintillator counters that were 5(10) cm thick. All counters were oriented horizontally except for a set of narrow vertical bars that were used to calibrate the horizontal coordinate measurement. A time-of-flight (ToF) resolution of 0.40 ns was achieved, and the coordinate resolution was 5 cm. The efficiency of each veto plane was found to be 97%. The detector was shielded on the target side with 5 cm of lead and 1 cm of iron and on all other sides with 5 cm of iron.

The trigger was formed using a 100 ns wide coincidence between the signals from BigHAND and BigBite, and required the total energy in the BigHAND scintillator counters to be above 25 MeV and the total energy deposited in the BigBite calorimeter to be above 500 MeV. A Monte Carlo of our experiment, that included a modeling of the detector response utilizing Geant4 [19], was found to be in good agreement with the detector characteristics obtained from the experimental data.

The BigBite spectrometer optics were used to reconstruct the momentum, direction, and the reaction vertex of the electrons. BigHAND was used to determine the direction and charge of the recoiling particle. Using BigBite, it was also possible to accurately determine the time at which the scattering event took place, which in turn provided the start time for computing the ToF of the recoil particles arriving in BigHAND, and hence the momentum, p_n, of the recoil nucleon. The three-momentum transfer, $\vec{q}$, was used to calculate, for the recoil nucleon, the missing perpendicular momentum, $p_\perp = |(\vec{q} - \vec{p}_n) \times \vec{q}|/|\vec{q}|$ and the missing parallel momentum, $p_\parallel = (\vec{q} - \vec{p}_n) \cdot \vec{q}/|\vec{q}|$. The invariant mass of the system comprised of the virtual photon and the target nucleon (assumed to be free and at rest), W, was calculated as $W = \sqrt{m^2 + 2\,m\,(E_i - E_f) - Q^2}$, where m is the neutron mass, E_i the beam energy, and E_f the energy of the detected electron. The identification of quasi-elastic events was largely accomplished using cuts on $p_\perp$ and W. Additional cuts included $p_\parallel$ and the total mass of the undetected hadrons, m_{un}. See Table II.

The measured asymmetry was calculated as:

$$A_{\text{meas}}^{p(a)} = \frac{1}{P_e\,P_{\text{He}}} \left[\frac{N_+^{p(a)} - N_-^{p(a)}}{N_+^{p(a)} + N_-^{p(a)}} \right], \qquad (1)$$

where $N_h^{p(a)}$ is the number of events (normalized to beam charge) with the target polarization parallel (antiparallel) to the vector of the holding magnetic field, and h is beam helicity. A statistically-weighted average of A_{meas}^p and A_{meas}^a, A_{meas}, was used in the g_n analysis. In the case of the elastic scattering of 100% longitudinally polarized electrons off 100% polarized free neutrons, in the one-photon approximation, g_n is related to the double spin asymmetry, A_{en}, through [20]

$$A_{en} = \frac{-2\sqrt{\tau(\tau+1)}\tan(\theta_e/2)\cos\phi^*\sin\theta^*(g_n/\mu_n)}{(g_n/\mu_n)^2 + \tau\left[1 + 2(1+\tau)\tan^2(\theta_e/2)\right]} +$$
$$\frac{-2\tau\sqrt{1+\tau+(\tau+1)^2\tan^2(\theta_e/2)}\tan(\theta_e/2)\cos\theta^*}{(g_n/\mu_n)^2 + \tau\left[1 + 2(1+\tau)\tan^2(\theta_e/2)\right]}, (2)$$

where $\tau = Q^2/4m^2$, θ^* is the angle between the neutron polarization vector, $\vec{P}_n$, and $\vec{q}$, and ϕ^* is the angle between the electron scattering plane and the $(\vec{P}_n, \vec{q})$ plane.

To obtain g_n from A_{meas} a number of corrections were applied, the most important of which are presented in Table II. A target dilution factor, D_t, was applied to account for scattering from the N_2 admixture in the target gas. Accidental coincidences were accounted for using a background dilution D_{bkgr} associated with an asymmetry

TABLE II: Data analysis parameters and the resulting asymmetry values used to calculate g_n (see text for details).

$\langle Q^2 \rangle$ [GeV^2]	1.72	2.48	3.41
W [GeV]	0.7-1.15	0.65-1.15	0.6-1.15
$p_\perp$ [GeV]	< 0.15	< 0.15	< 0.15
$p_\parallel$ [GeV]	< 0.25	< 0.25	< 0.40
m_{un} [GeV]	< 2.0	< 2.0	< 2.2
A_{meas}	-0.136	-0.134	-0.098
D_t	0.948	0.949	0.924
D_{bkgr}	0.970	0.981	0.975
A_{bkgr}	-0.001	-0.018	-0.012
A_{phys}	-0.148	-0.145	-0.109
D_{in}	0.980	0.963	0.851
A_{in}	-0.108	-0.254	-0.113
A_{QE}	-0.149	-0.141	-0.109
$D_{p/n}$	0.782	0.797	0.807
$\delta D_{p/n}$	0.022	0.033	0.042
A_{ep}	-0.010	-0.008	-0.006
$A_{en}|_{\text{exp}}$	-0.188	-0.175	-0.134

A_{bkgr} and were determined by considering the interval of the ToF spectrum that was free from real coincidence events. The resulting physical asymmetry, A_{phys}, was then corrected for inelastic single-pion electroproduction events, leading to the asymmetry for quasi-elastic processes, A_{QE}. The dilution from inelastic events, D_{in}, and the associated asymmetry, A_{in}, were calculated using our Monte Carlo, which employed the plane-wave impulse approximation (PWIA) along with the MAID parameterization [21]. The event yield in the Monte Carlo was normalized to match the data. In spite of its significant size, the inelastic background leads to only a small correction thanks to the observed asymmetry A_{phys} being close to A_{in}. The asymmetry $A_{en}|_{exp}$ was obtained from A_{QE} using the dilution factor $D_{p/n}$ and the asymmetry A_{ep} that accounted for the dilution in our final event sample from protons. This dilution was largely due to charge-exchange proton interactions in the shielding upstream of the veto planes. $D_{p/n}$ and its uncertainty $\delta D_{p/n}$ were computed by comparing data collected from three targets (H_2, ^{3}He, and N_2). The asymmetry A_{ep} was computed using the GEA calculations discussed below in a separate Monte Carlo.

The final steps in extracting g_n involve calculations of the asymmetries in the quasi-elastic processes $^3\overrightarrow{\text{He}}(\vec{e}, e'n)pp$ and $^3\overrightarrow{\text{He}}(\vec{e}, e'p)np$. These calculations were performed using the generalized eikonal approximation (GEA) [22], and included the spin-dependent final-state interactions and meson-exchange currents, and used the ^{3}He wave function that results from the AV18 potential [23]. The yield of the quasi-elastic events and the asymmetries were calculated as a function of W and assumed values of g_n with the values for the other nucleon FFs from [24]. The estimated accuracy of the GEA calculations is 2% [25]. The acceptance of the experimental setup, orientation of the target polarization, and the cuts applied to $p_\perp$ and $p_\parallel$ were all taken into account. We note that the effective neutron polarization for the cuts used on $p_\perp$ and $p_\parallel$, as calculated in the PWIA approximation, was greater than $\sim$96% of P_{He} (in agreement with [26]). The asymmetries for $^3\overrightarrow{\text{He}}(\vec{e}, e'n)pp$ calculated within GEA were found to be within 3% of the PWIA values, indicating that nuclear re-scattering effects were quite small. The experimental value of g_n and its statistical uncertainty were calculated by comparing $A_{en}|_{exp}$ with the asymmetries from the GEA calculations [25]. The systematic uncertainty was obtained by combining in quadrature the contributions of individual effects, as presented in Table III.

Our results for g_n are shown in Fig. 1 along with recent data sets that extend beyond Q^2=0.5 GeV^2 [5–8, 12]. It is important to compare our results with calculations that have described well the proton FF data. Three such calculations are shown in Fig. 1. In all of them, quark orbital angular momentum plays an important role. One is a logarithmic scaling prediction
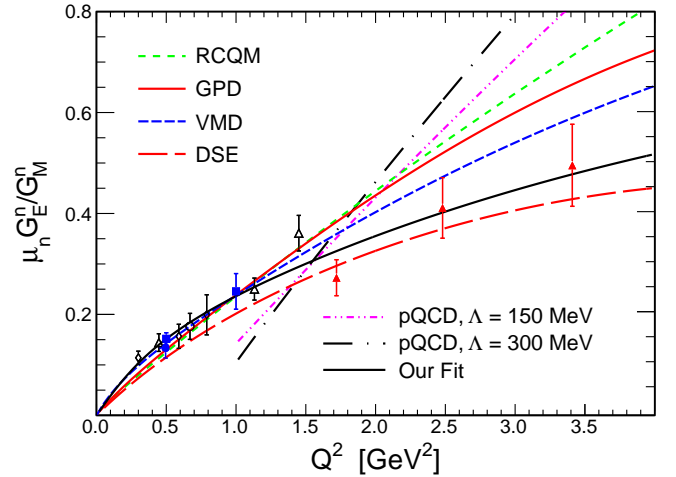

FIG. 1: The ratio of $\mu_n G_E^n/G_M^n$ vs. the momentum transfer with results of this experiment (solid triangles) and selected published data: diamonds [5], open triangles [6], circles [7], squares [8], open circles [12], and calculations: pQCD [27], RCQM [28], DSE [29], GPD [30], and VMD [31]. The curves labeled pQCD present pQCD-based scaling prediction [27] normalized to 0.3 at Q^2=1.5 GeV^2. The error bars for our data points show the statistical and the systematic uncertainties added in quadrature. Our fit is also shown; see parameterization in the text.

for the ratio of Pauli and Dirac nucleon form factors: $F_2/F_1 \propto \ln^2(Q^2/\Lambda^2)/Q^2$ [27], based on pQCD, which is shown for two values of the soft-scale parameter Λ. It is in clear disagreement with the combined neutron data, despite providing a good description of the proton data. The authors of [27] noted, however, that the agreement with the proton data may well have been due to delicate cancellations, given the relatively low values of Q^2 involved. Another calculation is the Light Front Cloudy Bag Model [28], an example of a relativistic constituent quark model (RCQM) calculation that, in this case, includes a pion cloud. Several RCQMs anticipated the observed decreasing Q^2 dependence of G_E^p/G_M^p. Finally, we show a calculation based on QCD's Dyson-Schwinger equations (DSE) [29], in which the mass of the quark propagators is dynamically generated. The calculation [29] is closest to our results. Also shown in Fig. 1 are predictions based on GPDs [30] and Vector Meson Dominance [31] that were fit to the data available prior to this work. Finally, our Galster-like fit to the 13 data points (used in Fig. 1) is shown by a solid black line: $g_n = \mu_n \left[a\tau/(1 + b\tau)\right] G_D/G_M^n$, where $G_D = 1/(1 + Q^2/(0.71\,\text{GeV}^2))^2$, G_M^n is from [24], and we find $a = 1.39$ and $b = 2.00$ with a total $\chi^2 = 7.8$.

Flavor-separated Dirac and Pauli FFs of the nucleon, $F_{1,2}^d$ and $F_{1,2}^u$ (for u and d in the proton), can be obtained from the electric and magnetic FFs of the proton and the neutron, assuming isospin symmetry and neglecting the contribution of the strange quark FFs [32]. Experimental data for g_n and the Kelly fit [24] for G_E^p, G_M^p, and G_M^n were used to compute the ratio F_1^d/F_1^u, shown in Fig. 2, which exhibits a downward trend with increasing Q^2.

TABLE III: Experimental results for $g_n \equiv \mu_n G_E^n / G_M^n$ and G_E^n (using linearly interpolated values of G_M^n from [35]), and also the contributions to the systematic uncertainty of G_E^n from individual sources (as a fraction of the G_E^n value).

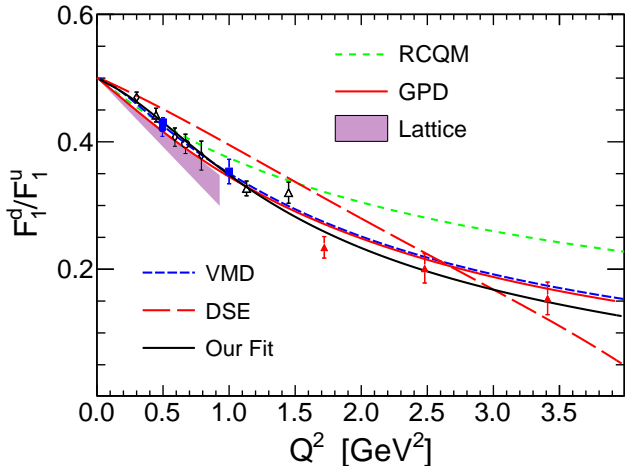| $\langle Q^2 \rangle$ [GeV^2]	$g_n \pm$ stat. $\pm$ syst.	$G_E^n \pm$ stat. $\pm$ syst.	G_M^n	P_{He}	P_n	P_e	$D_{p/n}$	D_{in}	other
1.72	$0.273 \pm 0.020 \pm 0.030$	$0.0236 \pm 0.0017 \pm 0.0026$	0.020	0.076	0.033	0.055	0.033	0.011	0.025
2.48	$0.412 \pm 0.048 \pm 0.036$	$0.0208 \pm 0.0024 \pm 0.0019$	0.024	0.059	0.024	0.031	0.036	0.027	0.023
3.41	$0.496 \pm 0.067 \pm 0.046$	$0.0147 \pm 0.0020 \pm 0.0014$	0.026	0.047	0.016	0.026	0.032	0.060	0.026

FIG. 2: Nucleon flavor FF ratio F_1^d/F_1^u vs Q^2. The band indicates the lattice QCD result [34]. Data and curves are the same as in Fig. 1.

This means that the corresponding infinite-momentum-frame charge density [33] of the d quark as a function of impact parameter is significantly broader than that of the u quarks. Such an experimental result could be related to the established decrease of the quark PDF ratio, d/u, with increasing x_{Bj}. The calculations discussed earlier, as well as the recent lattice QCD results [34], are in general agreement with experimental data for F_1^d/F_1^u.

We conclude by summarizing in Table III our experimental results. This experiment more than doubles the Q^2-range over which G_E^n is known, greatly sharpens the mapping of the nucleon's constituents and provides a new benchmark for comparison with theory.

* Corresponding author: bogdanw@jlab.org
† Deceased
[1] M.K. Jones et al., Phys. Rev. Lett. 84, 1398 (2000); O. Gayou et al., Phys. Rev. Lett. 88, 092301 (2002).
[2] S. Boffi and B. Pasquini, Riv. Nuovo Cim., 30, 387 (2007).
[3] X. Zheng et al., Phys. Rev. Lett. 92, 012004 (2004); A. Airapetian et al., Phys. Rev. Lett. 103, 152002 (2009).
[4] A.I. Akhieser, L.N. Rosenzweig, and I.M. Shmushkevich, Sov. Phys. JETP 6, 588 (1958); R.G. Arnold, C.E. Carlson, and F. Gross, Phys. Rev. C 23, 363 (1981).
[5] D.I. Glazier et al., Eur. Phys. J A 24, 101 (2005).
[6] B. Plaster et al., Phys. Rev. C 73, 025205 (2006).
[7] H. Zhu et al., Phys. Rev. Lett. 87, 081801 (2001);
[8] G. Warren et al., Phys. Rev. Lett. 92, 042301 (2004).
[9] C.E. Jones-Woodward et al., Phys. Rev. C 44, R571 (1991).
[10] J. Becker et al., Eur. Phys. J. A 6, 329 (1999).
[11] J. Golak et al., Phys. Rev. C 63, 034006 (2001).
[12] D. Rohe et al., Phys. Rev. Lett. 83, 4257 (1999); J. Bermuth et al., Phys. Lett. 564B, 199 (2003).
[13] W. Glöckle et al., Phys. Rep. 274, 107 (1996); H. Witala et al., Phys. Rev. C 63, 024007 (2001).
[14] R.J. Glauber, Phys. Rev. 100, 242 (1955).
[15] J. Alcorn et al., Nucl. Instrum. Methods Phys. Res., Sect. A 522, 294 (2004).
[16] W. Happer, G.D. Cates, M.V. Romalis, and C.J. Erickson, U.S. Patent No. 6,318,092 (2001); E. Babcock et al., Phys. Rev. Lett. 91, 123003 (2003).
[17] M.V. Romalis and G.D. Cates, Phys. Rev. A 58, 3004 (1998).
[18] D.J.J. de Lange et al., Nucl. Instrum. Methods Phys. Res., Sect. A 406, 182 (1998).
[19] S. Agostinelli et al., Geant4 Collaboration, Nucl. Instrum. Methods Phys. Res., Sect. A 506, 250 (2003).
[20] T.W. Donnelly and A.S. Raskin, Ann. Phys. (N.Y.) 169 247 (1986).
[21] D. Drechsel, S.S. Kamalov, and L. Tiator, Nucl. Phys. A645, 145 (1999) and Eur. Phys. J. A 34, 69 (2007).
[22] M.M. Sargsian et al., Phys. Rev. C 71, 044614 (2005).
[23] R.B. Wiringa et al., Phys. Rev. C 51, 38 (1995).
[24] J.J. Kelly, Phys. Rev. C 70, 068202 (2004).
[25] M.M. Sargsian, private communication (2010).
[26] J. Carlson and R. Schiavilla, Reviews of Modern Physics, 70(3), 743 (1998).
[27] A.V. Belitsky, X. D. Ji, and F. Yuan, Phys. Rev. Lett. 91, 092003 (2003).
[28] G.A. Miller, Phys. Rev. C 66, 032201(R) (2002); H.H. Matevosyan, A.W. Thomas, G.A. Miller, Phys. Rev. C 72, 065204 (2005); private communication (2009).
[29] C.D. Roberts et al., Eur. Phys. J. ST 140, 53 (2007); I.C. Cloët et al., Few-Body Systems 46, 1(2009).
[30] M. Diehl et al., Eur. Phys. J. C 39, 1 (2005); M. Guidal et al., Phys. Rev. D 72, 054013 (2005).
[31] E.L. Lomon, Phys. Rev. C 66, 045501 (2002); arXiv:nucl-th/0609020.
[32] G.A. Miller, B.M.K. Nefkens, and I. Slaus, Phys. Rep. 194, 1 (1990).
[33] G.A. Miller, Phys. Rev. Lett. 99, 112001 (2007).
[34] J.D. Bratt et al., arXiv:1001.3620.
[35] J. Lachniet et al., Phys. Rev. Lett. 102, 192001 (2009).